Origin and Segmental Diversity of Spinal Inhibitory Interneurons

Lora B. Sweeney[1], **Jay B. Bikoff**[2,*], **Mariano I. Gabitto**[3,*], **Susan Brenner-Morton**[2], **Myungin Baek**[4], **Jerry H. Yang**[1], **Esteban G. Tabak**[5], **Jeremy S. Dasen**[4], **Christopher R. Kintner**[1], and **Thomas M. Jessell**[2,6]

[1]Molecular Neurobiology Laboratory, Salk Institute for Biological Studies, La Jolla, CA 92037, U.S.A

[2]Howard Hughes Medical Institute, Zuckerman Institute, Depts. of Neuroscience, and Biochemistry and Molecular Biophysics, Columbia University, New York, NY 10032, U.S.A

[3]Center for Computational Biology, Flatiron Institute, Simons Foundation, New York, NY 10010, U.S.A

[4]Neuroscience Institute, Dept. of Neuroscience and Physiology, NYU School of Medicine, New York, NY 10016, U.S.A

[5]Courant Institute of Mathematical Sciences, New York University, New York, NY 10012, U.S.A

SUMMARY

Motor output varies along the rostro-caudal axis of the tetrapod spinal cord. At limb levels, ~60 motor pools control the alternation of flexor and extensor muscles about each joint, whereas at thoracic levels as few as 10 motor pools supply muscle groups that support posture, inspiration and expiration. Whether such differences in motor neuron identity and muscle number are associated with segmental distinctions in interneuron diversity has not been resolved. We show that select combinations of nineteen transcription factors that specify lumbar V1 inhibitory interneurons generate subpopulations enriched at limb and thoracic levels. Specification of limb and thoracic V1 interneurons involves the *Hox* gene, *Hoxc9*, independent of motor neurons. Thus, early Hox patterning of the spinal cord determines the identity of V1 interneurons and motor neurons. These studies reveal a developmental program of V1 interneuron diversity, providing insight into the organization of inhibitory interneurons associated with differential motor output.

Correspondence: lsweeney@salk.edu, mgabitto@simonsfoundation.org.
*These authors contributed equally.
[6]Lead Contact. tmj1@cumc.columbia.edu

Graphical abstract

Hox Patterning

Differential TF Expression

Segmental Inhibitory Interneurons

V1
V1^{Limb}
V1^{Thoracic}

Keywords

Inhibitory interneurons; spinal cord patterning; motor circuit; development; cell identity; transcription factor; Hox proteins

INTRODUCTION

The precision of movement in vertebrates is controlled by spinal cord neurons that elicit dynamic patterns of motor output that vary between species (Goulding, 2009). Agnathan and larval fish propel themselves forward via alternate contraction of axial musculature, resulting in undulatory movement. In contrast, tetrapods vary the precision and complexity of motor output along the rostro-caudal axis, with thoracic levels controlling trunk muscles for posture, inspiration and expiration, and limb levels regulating flexor and extensor muscle contractions for alternating joint movement. Such motor patterns emerge through the coordinated activity of excitatory and inhibitory interneurons that direct motor neuron firing. While the cardinal classes of interneurons that mediate spinal motor output are broadly conserved across evolution, the extent to which they vary along the body axis to support variant motor output has not been resolved (Grillner and Jessell, 2009).

The organization of motor neurons provides a framework for understanding how neural circuits become specialized for limb or thoracic motor output. Motor neurons differ in their molecular specification and positional segregation along the rostro-caudal axis of the spinal cord, in register with the identity of their muscle targets (Catela et al., 2015). At a first level of organization, motor neurons are spatially and molecularly subdivided into columns according to the region of the body they innervate. Motor neurons in the lateral motor column (LMC), located in brachial and lumbar spinal cord, innervate the fore- and hind-limbs, whereas those of the hypaxial (HMC) and preganglionic (PGC) motor columns at thoracic levels innervate body wall musculature and autonomic ganglia respectively, and those of the median motor column (MMC) innervate axial musculature (Dasen and Jessell, 2009). Beyond this columnar organization, motor neurons are subdivided into pools that innervate individual muscles, with the LMC and HMC containing approximately 60 and 10 motor pools respectively (Landmesser, 1978; Romanes, 1951; Smith and Hollyday, 1983).

These differences in motor neuron identity arise during rostro-caudal patterning of the spinal cord via the coordinated and cross-repressive interactions of *Hox* genes — each of which is expressed over a restricted segmental domain. In the brachial spinal cord, for instance, Hoxc6 is expressed by and promotes the expression of FoxP1 and retinoic acid in most motor neurons that innervate muscles in the fore- and hind-limbs (Dasen et al., 2008; 2003; Mendelsohn et al., 2017; Rousso et al., 2008). In contrast, at thoracic levels, the expression of Hoxc9 represses Hoxc6 and limb identity, resulting in the formation of hypaxial and preganglionic motor columns (Baek et al., 2017; Jung et al., 2010). Within each column, ensembles of motor neurons that connect to individual muscles are further clustered into motor pools, each defined by the combinatorial expression of Hox-family and other downstream transcription factors (Dasen et al., 2005; De Marco Garcia and Jessell, 2008; Friese et al., 2009; Lin et al., 1998). These differences in columnar and pool-specific transcription factor expression dictate motor neuron identity, axon trajectory and peripheral target connectivity (Dasen and Jessell, 2009).

At all segmental levels, ventral spinal interneurons fall into four cardinal classes, termed V0 to V3 neurons, which arise from different ventral progenitor domains and give rise to interneurons with distinct settling position, neurotransmitter expression, and profiles of connectivity (Grossmann et al., 2010). Within each cardinal class, molecularly, anatomically, and physiologically distinct interneuron subpopulations have been identified (Bikoff et al., 2016; Zagoraiou et al., 2009). By comparison, how the identity and distribution of these diverse interneuron classes varies to accommodate rostro-caudal differences in motor neuron number and identity is largely unexplored. The core molecular and physiological identities of interneuron subtypes may be preserved at different rostro-caudal levels but rewired to accommodate differences in motor output. Alternatively, level-specific interneuron subtypes, each marked with a specialized molecular code, might operate at limb and thoracic levels. Spinal interneuron diversity at limb and thoracic levels of the spinal cord has been examined previously (Francius et al., 2013), but without the emergence of prominent distinctions in segmental identity.

The V1 inhibitory population comprises over one third of all ventral inhibitory interneurons, and for two reasons is an appealing candidate for examining variations in identity along the

rostro-caudal axis (Zhang et al., 2014). First, it contains a well-defined subpopulation of reciprocal interneurons that contribute to flexor-extensor alternation of limb muscles, a feature absent at thoracic levels (Benito-Gonzalez and Alvarez, 2012; Jankowska and Odutola, 1980; Sears, 1964; Zhang et al., 2014). Second, V1 interneurons exhibit striking molecular diversity at lumbar levels, comprising ~50 candidate cell types that emerge primarily from four clades and express a variable combination of 19 transcription factors that segregate with neuronal settling position, physiology and differential connectivity (Bikoff et al., 2016; Gabitto et al., 2016). The existence of extensive molecular diversity in lumbar V1 interneurons raises the question of whether their diversification matches motor neuron subtype identity at brachial, lumbar and thoracic levels of the spinal cord.

We have considered whether V1 interneurons are organized along the rostro-caudal axis into molecularly distinct subpopulations, to accommodate the differential motor outputs of limb and torso. We examined the variation in number and diversity of V1 interneurons at thoracic compared to lumbar levels of the spinal cord. Thoracic V1 interneurons express the same 19 transcription factors and segregate into the same 4 clades as at lumbar levels. While singly, none of these 19 V1 subclass markers distinguishes segmentally restricted interneurons, pairwise or triplet combinations reveal limb- and thoracic-specific V1 subpopulations. We then show that limb- and thoracic-specific differences in V1 interneurons emerge through a Hox-dependent mechanism in which Hoxc9 determines the distinction between brachial and thoracic V1 interneurons. Notably, the segmental identity of V1 interneurons is unaffected by the absence of motor neurons, arguing for independent Hox control of motor neuron and interneuron fates. The existence of segment-specific V1 interneuron subpopulations provides insight into how inhibitory interneurons are specialized for variant motor output at limb and thoracic levels of the spinal cord.

RESULTS

Comparison of Lumbar and Thoracic V1 Interneuron Subpopulations Defined by Single Transcription Factor Expression

To explore how inhibitory interneuron diversity varies along the rostro-caudal axis of the spinal cord, V1 interneurons — genetically marked by *En1::Cre* driven expression of a *Tau.lsl.nLacZ* reporter (*En1.nLacZ*) — were profiled at the thoracic and lumbar levels of the p0 spinal cord by labeling with one of 19 transcription factors, each chosen based on its expression in lumbar V1 interneurons at p0 (Bikoff et al., 2016; Figure 1A).

At thoracic levels, the spinal cord is 30% thinner in width (Figure 1B) and has two-fold fewer motor neurons (Agalliu et al., 2009; Dasen et al., 2008; Rousso et al., 2008). This general scaling of ventral neuronal cell types along the rostro-caudal axis was also found for V1 interneurons, with approximately half the total number of neurons at thoracic levels as in an equivalent section at lumbar levels (49 ± 2.1 thoracic versus 107 ± 4.2 lumbar V1 interneurons per 12 μm hemi-section, respectively; Figure 1B). To correct for this difference in total V1 neuronal number, we compared the percentage of *En1.nLacZ*[+] V1 interneurons expressing each of the 19 transcription factors (V1[1TF]) at thoracic and lumbar levels and found 18/19 V1[1TF] subpopulations were similar in proportion at lumbar and thoracic levels, with the exception of V1[Pou6f2], which was two-fold enriched at lumbar levels (Figure 1C,

S1A). Thus, all 19 transcription factors that demarcate V1 subpopulations in the lumbar spinal cord are also expressed in subpopulations of thoracic V1 interneurons in similar proportions, indicating that V1 subpopulations cannot be segmentally restricted on the basis of expression of these single transcription factors.

We next asked whether $V1^{1TF}$ subpopulations acquire different settling positions along the dorso-ventral and medio-lateral axes in the thoracic versus lumbar spinal cord, as settling position has been demonstrated to correlate with an interneuron's innervation pattern and functional identity (Benito-Gonzalez and Alvarez, 2012; Bikoff et al., 2016; Figure 1D–E). Since the overall shape of the spinal cord differs along the medio-lateral axis between levels, we transformed each thoracic cell's position along this axis into its lumbar equivalent mathematically using a linear transformation (Figure S1B). Following this shape normalization, we quantified the average distance (μ) that a $V1^{1TF}$ interneuron at thoracic levels needs to be displaced to represent the corresponding $V1^{1TF}$ interneuron subpopulation at lumbar levels (Figure S1B and Methods S1). This value enabled the comparison of spatial distributions, permitting each $V1^{1TF}$ interneuron subpopulation to be ranked according to similarity (Figure 1D and S1C). The three $V1^{1TF}$ subpopulations with the largest displacement values exhibited clear differences in position between segmental levels (Figure 1E), suggesting the appearance of level-specific subpopulations within the parental population.

These findings indicate that V1 interneuron diversity marked by single transcription factor expression is remarkably conserved at different segmental levels. Total V1 interneuron number scales to motor neuron number on average, and in most instances each $V1^{1TF}$ interneuron subpopulation largely occurs in a similar proportion and settles in a similar relative position along the dorso-ventral and medio-lateral axes at thoracic and lumbar levels. Despite this conservation, $V1^{1TF}$ interneurons can be detected at lumbar and thoracic levels that differ in the fraction of cells that express a given transcription factor (e.g. $V1^{Pou6f2}$), or in settling position along the medio-lateral (e.g. $V1^{Pou6F2}$) or dorso-ventral (e.g. $V1^{Prdm8}$) axes. These differences raise the possibility that segmentally-restricted V1 subpopulations may be revealed through an analysis of combinatorial expression of more than one transcription factor.

Combinatorial Expression of Two Transcription Factors Reveals Limb- and Thoracic-enriched V1 Interneuron Subpopulations

To ascertain whether more refined subsets within the parental V1 population segregate along the rostro-caudal axis, we scored the number and settling position of genetically-marked V1 interneurons co-expressing two transcription factors ($V1^{2TF}$) at lumbar and thoracic spinal segments of p0 mice (Figure 2A). Of the transcription factors that were co-expressed, the majority of $V1^{2TF}$ combinations we tested (54/65, or 83%) labeled a similar percentage of V1 interneurons at thoracic and lumbar segments, with less than two-fold differences between these segmental levels (Figure S2A). The remaining 11 $V1^{2TF}$ combinations exhibited at least two-fold enrichment at one level versus the other, with subsets of V1 interneurons detected selectively at thoracic ($V1^{Otp+Sp8}$) or lumbar ($V1^{Oc1+Pou6f2}$ or $V1^{Oc2+Pou6f2}$) levels (Figure 2B).

Further analysis of thoracic V1^{2TF} settling positions revealed highly restricted spatial distributions compared to V1^{1TF} subpopulations. For example, V1^{Prdm8} neurons at both thoracic and lumbar levels exhibit bimodal distributions, yet show strong biases toward either a dorsal or ventral position within an individual segment (Figure 2C). These positional biases correspond to transcriptionally delineated subsets defined by co-expression of a second transcription factor, exemplified by Foxp2, which labels the ventral lumbar V1^{Prdm8} subpopulation, and Otp, which labels the dorsal thoracic V1^{Prdm8} subpopulation (Figure 2D–E). Even amongst V1^{2TF} subpopulations that labeled a similar percentage of lumbar and thoracic V1 interneurons, segment-specific biases in settling position were evident (Figure S2B). Subdividing V1 interneurons by the co-expression of two transcription factors therefore reveals V1 diversity that differs markedly along the rostro-caudal axis of the spinal cord, and suggests potential diversity based on the expression of more than two transcription factors.

Segmental V1 Diversity Associated with Fore- and Hind-limbs

Four of the V1^{2TF} subpopulations with the most segmental enrichment and largest size were examined further in the brachial (fore-limb level) spinal cord. The V1 interneuron population as a whole was similar in size and position at brachial and lumbar levels (Figure 3A). Two thoracic-enriched V1^{2TF} subpopulations, the proportionately enriched V1$^{FoxP2+Nr4a2}$ or the near exclusive V1$^{Otp+Sp8}$, were similarly absent or greatly reduced at brachial levels, consistent with these two V1 subpopulations operating in the context of thoracic motor circuitry (Figure 3B–C). Conversely, two lumbar-enriched V1^{2TF} subpopulations, V1$^{FoxP4+Prdm8}$ and V1$^{Lmo3+Pou6f2}$, were also enriched at brachial levels, suggesting they operate in the context of local circuits present at both fore- and hind-limb levels (Figure 3D–E). Moreover, the settling position of each population was similar at brachial and lumbar levels, consistent with each representing V1 interneurons conserved across limb levels (Figure 3D–E). Together these data suggest that the segmentally restricted V1 subpopulations we identify correspond to limb versus non-limb motor distinctions. We note however, that a survey of eight V1^{1TF} subpopulations at brachial and lumbar levels reveals largely identical V1 proportions (Figure S3A), but occasionally distinct settling positions (Figure S3B), suggesting that additional V1 diversity may be uniquely associated with hind- versus fore-limb.

We further evaluated these four limb- and thoracic- V1^{2TF} interneuron subpopulations both early and late during spinal circuit maturation to assess the stability of marker expression and segment specificity over developmental time. At e14.5, shortly after the end of V1 interneuron neurogenesis (Benito-Gonzalez and Alvarez, 2012; Stam et al., 2012), three of four segmentally restricted expression patterns were evident, suggesting that these distinctions are specified early (Figure S3C). Later at p21, when V1 synaptic connections have formed and stabilized, the level-specific co-expression of these four marker combinations largely persisted with the exception of FoxP4, which was down-regulated (Figure S3C). The subpopulations we identify thus are specific to a segmental level, and not a given developmental stage.

We next asked whether these V1 interneuron subpopulations varied within each segmental level. The two limb-enriched subpopulations, V1$^{Lmo3+Pou6f2}$ and V1$^{FoxP4+Prdm8}$, were enriched in the posterior (L3-5) compared to anterior (L1-2) lumbar spinal cord (Figure S3D). The two thoracic-enriched subpopulations also were differentially distributed in the thoracic spinal cord — with V1$^{Otp+Sp8}$ most enriched at T7-9 and V1$^{FoxP2+Nr4a2}$ evenly distributed from T1-12 (Figure S3D). While such rostro-caudal variation between segments of each limb or thoracic subpopulation could reflect differences in connectivity with specific motor pools, the underlying logic of the interneuron diversity we identify is associated with the fore- and hind-limb.

Bayesian Modeling of V1 Thoracic Diversity

To characterize systematically the extent of cell type diversity within thoracic V1 interneurons, we extended a Bayesian statistical model that was used previously to define the number and transcription factor expression profile of candidate V1 cell types at lumbar levels, to thoracic spinal cord levels (Gabitto et al., 2016). Three data sets served as input for this Bayesian analysis: the fraction of thoracic V1 interneurons that express each of 19 transcription factors, the fraction of thoracic V1 interneurons that express binary combinations of 19 transcription factors, and the settling position of each thoracic V1^{1TF} interneuron population (Figure 4A; see also Figures 1 and S1 and Methods S1).

This analysis identified 60 candidate thoracic cell type expression profiles, each of which was defined by the combinatorial expression of 2 to 11 transcription factors (mean ± SD: 4.6 ± 0.1 transcription factors per cell type; Figure 4B), and predicted that, on average, a set of 38 candidate thoracic V1 cell types best explained the data (mean ± SD: 38.33 ± 1.38; Figure 4C). To validate the computational model of thoracic V1 diversity, we assessed the model's ability to predict accurately the prevalence of inferred cell types. We focused on the fraction of V1 interneurons simultaneously expressing 3 transcription factors within the Sp8 and FoxP2 clades, which contain the majority of thoracic V1 diversity. For the majority of V1^{3TF} combinations (72/91, or ~80%), the inferred fractional values were in good agreement with the measured values (Figure S4A).

We next compared our estimates of V1 diversity at thoracic and lumbar levels. The average number of candidate thoracic cell types was somewhat lower than the lumbar estimate (38 thoracic versus 50 lumbar candidate cell types), yet revealed that both limb and non-limb levels of the spinal cord exhibit a high degree of inhibitory interneuron diversity. Moreover, the average number of transcription factors expressed in candidate thoracic and lumbar V1 cell types was similar (4.6 ± 0.1 transcription factors at thoracic levels v. 4.0 ± 1 transcription factors at lumbar levels).

We arranged the most prevalent predicted set of candidate cell types at each level (mode of the posterior, see STAR Methods and Methods S1) into hierarchical and mutually exclusive clades to compare the organizational logic of lumbar and thoracic diversity (Figure 4D–H; see Gabitto et al., 2016). As at lumbar levels, the absence of co-expression subdivided V1 interneurons in the thoracic spinal cord into 4 clades encompassing the transcription factors V1^{FoxP2}, V1^{MafA}, V1^{Pou6f2}, and V1^{Sp8} and comprising greater than 50% of all thoracic V1 interneurons (see Gabitto et al., 2016 for more detail). Within each of the four clades the

organization was almost perfectly conserved up to and, in some cases, beyond the second hierarchical level (Figure 4D–H, bold lines). Furthermore, the relative size of each clade and the core set of transcription factors expressed within a clade were comparable between lumbar and thoracic levels (Figure 4D–H). Together, these results support the existence of a conserved underlying logic defining cell type diversity along the rostro-caudal axis of the spinal cord.

Despite these similarities, notable differences in thoracic and lumbar cell type diversity were evident. In some cases, this divergent diversity emerged from the expression of new transcription factors within clades, exemplified by Prdm8 in the lumbar FoxP2 clade (Figure 4F) and Otp and Nr3b3 in the thoracic Sp8 clade (Figure 4G). In other cases, differences emerged from variant combinations of transcription factors that mark the same proportion of V1 interneurons at both levels but exhibit level-specific variations in position (Figure 1 and S1). This mechanism for generating additional cell type diversity using shared transcription factors was evident within the Pou6f2 clade (Figure 4E). At lumbar levels, MafB and Nr5a2 were co-expressed by a single candidate $V1^{Pou6f2+Zfhx4}$ cell type, while at thoracic levels, MafB and Nr5a2 were mutually exclusive in their expression, generating two candidate cell types. Similarly, within the FoxP2 clade, subsets of shared transcription factors differed in their co-expression at each segmental level: while MafB, Bhlhb5, and FoxP1 were present in the FoxP2 clade at both levels, they were co-expressed with FoxP4 and Lmo3 at lumbar levels, and Otp and Nr3b3 at thoracic levels (Figure 4F). These instances demonstrate the potential of combinatorial transcription factor expression to drive diversification in the absence of a level-specific transcription factor.

To assess the extent of transcriptional differences at thoracic and lumbar levels quantitatively, we counted the number of cell types expressing identical transcription factor combinations in the most common predictive cell type distribution of the Bayesian model (mode of the posterior, see Figure S4B, STAR Methods and Methods S1). Within the most prevalent set, we found that only 4 candidate cell types shared identical expression profiles between thoracic and lumbar spinal segments: $V1^{MafA+MafB+Oc2+Zfhx4+Oc1}$, $V1^{FoxP2+Nr3b2+Otp+Lmo3}$, $V1^{Sp8+Oc2+Lmo3}$ and $V1^{Sp8+Prdm8+Prox1+Lmo3}$ interneurons (Figure 4D–H and S4B). We expanded this analysis to include all candidate cell types predicted by the algorithm with 95% confidence, and similarly found few were shared between levels (10 of 158; data not shown). Interestingly, the transcriptional profile of one of these candidate cell types, $V1^{MafA+MafB+Oc2+Zfhx4+Oc1}$, mirrors that of a Renshaw cell (Stam et al., 2012), which is known to exist at all spinal cord levels (Benito-Gonzalez and Alvarez, 2012; Kirkwood et al., 1981).

Given relatively few identical candidate cell types, we sought to gain insight into the nature of the combinatorial code that distinguishes the majority of cell types at each level. We quantified the extent of transcriptional differences between thoracic and lumbar candidate cell types by determining the average number of transcription factors that differ between each lumbar and thoracic predicted cell type (see Methods S1). This analysis found an average difference of two transcription factors between any thoracic candidate cell type and the lumbar one of greatest similarity, supporting the idea that segment-specific diversity

arose from the variant co-expression or repression of a few differentially appropriated transcription factors.

To examine the extent of combinatorial diversity generated by transcription factors common to both levels, we compared the segmental enrichment of computationally predicted and experimentally measured $V1^{3TF}$ subsets. We identified 65 $V1^{3TF}$ combinations, defined by the presence or absence of FoxP2 or Sp8 expression and two additional transcription factors that were amenable for experimental measurement due to antibody compatibility. Of these 65 $V1^{3TF}$ combinations, 15 had a predicted thoracic or lumbar enrichment of two-fold or greater, and 10 of 15 (~70%) were validated immunohistochemically, demonstrating that a third transcription factor can generate further segmental diversity (Figure S4C).

Three examples best demonstrate how our measured $V1^{3TF}$ proportions validated our predictions of their segmental enrichment (Figure S4D–F). First, the model predicted and we confirmed that the presence or absence of Prdm8 expression further subdivided the thoracic-specific $V1^{Sp8+Otp+}$ subpopulation into two smaller subpopulations (Figure S4D). Second, within the FoxP2 clade, the model predicted, and we validated experimentally, that expression of FoxP1 defined a lumbar-specific subpopulation within the evenly distributed $V1^{FoxP2+Nr3b2+}$ subpopulation (Figure S4E) and third, lack of Otp expression defined a thoracic-specific subpopulation within the enriched $V1^{FoxP2+Nr4a2+}$ subpopulation (Figure S4F). These three examples demonstrate how a third transcription factor can further subdivide V1 interneurons into segment-specific subpopulations in agreement with predicted differences in cell type diversity.

This detailed analysis of candidate cell type prevalence validates the concept of segment-specific V1 interneuron diversity, generated by a multi-transcription factor combinatorial code. Such differences in transcriptional identity imply specialized interneurons exist at thoracic and lumbar levels of the spinal cord, in register with the thoracic-specific hypaxial and preganglionic, and the limb-specific lateral, motor columns.

Mechanism of Patterning of V1 Interneurons Along the Rostro-caudal Axis

We next explored the developmental mechanisms by which V1 interneurons acquire segment-specific identities. The appearance of V1 interneuron segmental identity at e14.5 (Figure S3C) suggests that V1 interneurons are specified, like motor neurons, early in development, rather than or perhaps in addition to, selective loss or addition of V1 interneuron subpopulations or marker co-expression at different segmental levels later during circuit maturation.

Hox transcription factors, a critical determinant of motor neuron rostro-caudal identity, might similarly play a role in specifying segmental interneuron identity. In brachial motor neuron progenitors, Hoxc6 promotes high-level expression of Foxp1, a critical step in specifying motor neurons that occupy the lateral motor column (LMC) and innervate limb musculature (Dasen et al., 2003; 2008; Lacombe et al., 2013). At thoracic levels, Hoxc9 acts to specify the HMC and PGC, respectively, by suppressing Hoxc6 and Foxp1 expression (Jung et al., 2010; 2014). Accordingly, Hoxc9 mutant mice show an expansion of Hoxc6

into the thoracic spinal cord, thereby suppressing thoracic motor neuron specification and inducing an ectopic LMC (Jung et al., 2010).

We first determined whether Hox genes were expressed within differentiating V1 interneurons. The potent regulator of thoracic identity, Hoxc9, is known to be expressed by interneuron progenitors at thoracic levels (Dasen et al., 2003). Moreover, we found that Hoxc9 and Hoxc6 were expressed in all differentiating thoracic and brachial V1 interneurons respectively at e14.5 (Figure S5A). Additionally, we observed the level-specific Hox paralogues, Hoxa10 and Hoxd10, are expressed in lumbar V1 interneurons at p0 (Figure S5B). These observations are consistent with a potential Hox involvement in V1 interneuron differentiation along the rostro-caudal axis.

To determine whether limb- and thoracic-enriched V1 subpopulations emerge through a Hox-dependent mechanism, we examined V1 interneuron identity in $Hoxc9^{-/-}$ mice (McIntyre et al., 2007). In thoracic spinal segments of e14.5 $Hoxc9^{-/-}$ mice, Hoxc9 expression was lost and Hoxc6 expression gained (Figure 5A), and thoracic motor neurons adopted an LMC-like identity, characterized by FoxP1 and Raldh2 expression (Figure 5B). To evaluate segmental interneuron identity in $Hoxc9^{-/-}$ mice, we exploited the finding that the limb-specific combination of Prdm8 and FoxP4, and the thoracic-specific combination of Otp and Sp8, each mark a near identical neuronal subpopulation with or without a V1 lineage trace (Figure S5C).

In control animals at e18.5, Prdm8+FoxP4+ neurons were enriched at brachial and lumbar compared to thoracic levels, whereas Otp+Sp8+ neurons were enriched at thoracic levels and largely absent from the brachial and lumbar spinal cord. In $Hoxc9^{-/-}$ mutants, the rostro-caudal distribution of segmental V1 interneurons was inverted — Prdm8+FoxP4+ neurons appeared in (Figure 5C) and Otp+Sp8+ neurons largely disappeared from the thoracic spinal cord (Figure 5D), while in the brachial spinal cord, their cell number was unaffected (Figure 5C–D).

Together these results show a consistent transformation of V1 markers in $Hoxc9^{-/-}$ mutants from thoracic- to limb-like, indicating that similar to motor neurons, V1 interneurons are segmentally restricted based on early Hox patterning along the rostro-caudal axis of the spinal cord.

V1 Segmental Identity Is Maintained in the Absence of Motor Neurons

The rostro-caudal distribution of V1 interneuron subpopulations in $Hoxc9^{-/-}$ mice raised the question of how Hoxc9 functions to promote rostro-caudal differences in V1 interneurons. Hoxc9 could act indirectly by changing the segmental identity of motor neurons, which are born prior to V1 interneurons and produce segment-specific differentiation cues such as retinoic acid, a secreted signal known to regulate Hox expression and the fate of motor neurons (Sockanathan and Jessell, 1998; Sockanathan et al., 2003). Alternately, Hoxc9 could act directly in V1 progenitors or newly post-mitotic neurons to specify segmental identity in a cell autonomous manner. This latter possibility is supported by the known function of many Hox genes in autonomously specifying motor and hindbrain neuronal identity (Philippidou and Dasen, 2013).

To distinguish between these two possibilities, we examined V1 interneuron diversity in *Olig2*$^{-/-}$ mutant mice, where motor neuron formation is abolished (Dessaud et al., 2007; Novitch et al., 2001; Rousso et al., 2008). The loss of motor neurons in *Olig2*$^{-/-}$ mutants was confirmed with the motor neuron marker Hb9 and the LMC markers FoxP1 and Raldh2, both of which were absent from *Olig2*$^{-/-}$ mice at e14.5 (Figure 6A–D). To label segment-specific V1 subpopulations in *Olig2*$^{-/-}$ mice, we again used the limb-specific transcription factor combination of Prdm8 and FoxP4 and the thoracic-specific, Otp and Sp8 (Figure S5C). At brachial, thoracic and lumbar levels, the percentage of V1 interneurons expressing these markers was unchanged in *Olig2*$^{-/-}$ mutant mice (Figure 6E–F). The positioning of these V1 subpopulations was altered in *Olig2*$^{-/-}$ mutants, likely a consequence of the change in the shape of the spinal cord when motor neurons are absent. These results indicate that the early specification of V1 interneuron subpopulations occurs in the absence of motor neurons.

Our study demonstrates that V1 interneurons, like motor neurons, have limb- and thoracic-associated subpopulations (Figure 7). At brachial and lumbar levels of the spinal cord, limb-innervating LMC motor neurons and limb-specific inhibitory V1 interneurons, and at thoracic levels, hypaxial and preganglionic motor neurons and thoracic-specific V1 interneurons, form transcriptionally and spatially distinct subpopulations. These rostro-caudal patterns of V1 interneurons are Hox-dependent (Figure 7B), but motor neuron-independent (Figure 7C).

DISCUSSION

The emergence of limbs in terrestrial vertebrates necessitated changes in the organization of spinal circuits, best exemplified by the addition of limb-innervating motor neurons in the lateral motor column. Whether and how the network of interneurons that control motor output similarly changed to accommodate limb-based movement has been unclear. Here, we examined whether the identity of a coherent population of interneurons differs between limb and non-limb levels, through molecular profiling of V1 inhibitory interneurons along the rostro-caudal axis of the mouse spinal cord.

We find that V1 interneurons exhibit segment-specific subpopulations, revealed by differences in the combinatorial expression of transcription factors. The segmental identity of V1 interneurons is transformed in *Hoxc9*$^{-/-}$ mutants in which the thoracic spinal cord becomes limb-like, supporting the idea that these molecularly identified populations serve segmentally restricted functions. Furthermore, the molecular identity of segmentally restricted V1 interneurons is established independently of motor neurons. *Hox* genes therefore appear to act autonomously and independently to regulate interneuron and motor neuron identity, thus specifying components of spinal motor microcircuitry in a segment-selective manner.

Combinatorial Transcription Factor Expression Distinguishes Segmental Inhibitory Interneurons

Our analysis supports the view that substantial similarity exists in the logic of V1 interneuron diversification along the rostro-caudal axis of the spinal cord. At all spinal cord

levels, the most prominent feature preserved is the clade logic. Not only are 18 of 19 transcription factors expressed in similar proportions within thoracic V1 interneurons, but the V1 population as a whole can be subdivided into the same four non-overlapping clades — FoxP2, MafA, Pou6f2, and Sp8. Within each clade, a similar subset of transcription factors is expressed by thoracic and lumbar V1 interneurons. This finding implies strong conservation in aspects of V1 transcriptional identity along rostro-caudal axis, conferring the same proportion and pattern of V1 interneurons expressing each of 19 transcription factors, regardless of regional character.

However, evaluation of the number, overlap, and settling position of interneurons expressing at least two transcription factors revealed variation in V1 diversity in different segments of the spinal cord. These differences were first apparent in V1 subpopulations that express two transcription factors and became more pronounced in even smaller V1 subsets that express three or more transcription factors. Computational modeling, which predicts ~50 lumbar and ~38 thoracic cell types, indicates a similar degree of diversity, despite the differences in motor pool number. Notably, few transcriptionally identical V1 cell types were found at limb- and non-limb levels, raising the possibility that the molecular identity of limb- and non-limb associated V1 interneurons differs substantially in register with distinctions in motor output.

These data lead us to propose that V1 interneurons share a common cladistic logic of transcription factor expression that likely confers shared cellular properties, but nevertheless, differ in the expression of transcription factors that generate segmental identity. This mechanism may be relevant to other brain regions. A combinatorial transcription factor code that generates diversity in an entire population could be varied further to produce additional diversity in a region-specific manner. Indeed, recent studies have shown remarkable heterogeneity in other interneuron populations, where cell type diversity largely results from changing the expression of not one but rather a combination of genes (Cadwell et al., 2016; Campbell et al., 2017; Tasic et al., 2016; Wallace et al., 2017; Zeisel et al., 2015).

Hox Genes and the Emergence of Limb and Thoracic V1 Diversity

The finding that V1 interneurons differ in their molecular profile along the rostro-caudal axis raises the question of how such differences emerge during development. One simple mechanism would be to employ motor neurons as a source of segmentally restricted specification cues. At the time of V1 interneuron differentiation between e9.5 and e12.5 (Benito-Gonzalez and Alvarez, 2012; Stam et al., 2012), limb-innervating motor neurons within the LMC have acquired a columnar identity and are known to secrete a potent differentiation cue that controls spinal Hox gene expression, retinoic acid (Sockanathan et al., 1998) — making them an attractive candidate for non-autonomous segmental cues. Nevertheless, our experiments demonstrate that V1 interneurons do not require motor neurons to establish limb- and thoracic-specific subtypes, since segmental-specific identity is not perturbed in *Olig2*$^{-/-}$ mice that lack spinal motor neurons.

We instead find that Hox proteins specify the molecular character of V1 interneurons along the rostro-caudal axis of the spinal cord, mirroring the role of *Hox* genes in motor neuron specification. Segmental V1 interneuron identity is specified by the master regulator of

thoracic motor neuron identity, Hoxc9, thus providing a molecular means to coordinate the development of segmental identity in two interconnected neuronal populations within the same circuit. These molecular differences are present as early as e14.5 and persist until p21 (Figure S3C), suggesting they arise prior to the period of interneuron apoptosis and initial synapse formation, and are sustained until after synapse maturation and stabilization. Thus, it is unlikely that segmental-specific interneuron identity emerges from selective death of particular neuronal subsets or from patterned neural activity.

Within each segment, motor neurons are further diversified into pools that each innervate a single muscle through the coordinated and cross-repressive interaction of Hox paralogues and Meis TALE family co-factors (Dasen et al., 2005; Lacombe et al., 2013). As in motor neurons, we find differential Hox paralogue expression in V1 interneurons at each segmental level — with Hoxc4, c6, and a5 expressed rostrally at brachial levels (Figure S5A and data not shown), and Hoxa10 and d10 caudally at lumbar levels (Figure S5B). We propose that the combinatorial expression of these segment-specific Hox paralogues, potentially in combination with other Hox co-factors, further subdivides V1 interneurons at each segmental level into smaller, spatially and transcriptionally distinct subpopulations, thus generating limb- and thoracic- specific V1 interneuron diversity, in the same way that combinatorial and cross-repressive interactions between *Hox* genes in motor neurons lead to the generation of segment-specific motor pools.

Segmental V1 Diversity and Motor Coordination

Our experiments are consistent with the idea that V1 interneuron diversity is correlated with the limb or thoracic motor circuits they subserve. The V1 subtypes specific to lumbar levels are also found in the same number and settling position at brachial levels of the spinal cord. Conversely, thoracic-specific subtypes are essentially absent from both lumbar and brachial levels. Moreover, we find that $Hoxc9^{-/-}$ mutant mice exhibit ectopic limb-like V1 interneurons at thoracic levels, in register with the parallel emergence of ectopic LMC motor neurons. This coordinate specification of motor neuron and inhibitory interneuron identity suggests that their molecular signatures reflect a need to accommodate segment-specific circuit functions.

Prior studies of interneuron physiology have identified functional subsets of inhibitory interneurons associated with limb movement. Unlike trunk muscles, the joints of the limb exhibit reciprocity in flexor and extensor muscle activation, which results from the activation of Ia reciprocal inhibitory neurons present at limb but not thoracic levels of the spinal cord (Jankowska and Odutola, 1980; Sears, 1964). These group Ia reciprocal inhibitory interneurons arise from a combination of both the V1 and V2b cardinal classes of interneurons (Eccles and Lundberg, 1958; Hultborn et al., 1971; Zhang et al., 2014), yet their precise molecular identity remains unclear. The transcription factor FoxP2 has been suggested to define the V1 subset of Ia reciprocal interneurons (Benito-Gonzalez and Alvarez, 2012), but its relatively broad distribution in the ventral spinal cord suggests it may not be a selective marker for Ia inhibitory interneurons, which occupy a relatively restricted ventrolateral domain within Rexed lamina VII (Alvarez et al., 2005; Benito-Gonzalez and Alvarez, 2012; Hultborn et al., 1971). Here, we identify a limb-specific and ventrolateral

subtype defined by the coincident expression of FoxP2, FoxP4, and Prdm8, a possible molecular signature of Ia-inhibitory neurons in the V1 lineage. This transcription factor profile suggests that reciprocal inhibitory connectivity and function may be genetically encoded.

In contrast to reciprocal inhibitory circuits that operate solely at limb-levels, recurrent inhibition of motor neurons exists at all rostro-caudal levels of the spinal cord (Eccles et al., 1954; Kirkwood et al., 1981; Lipski et al., 1985; Renshaw, 1941). Consistent with this observation, we identify a candidate V1 cell type at thoracic and lumbar levels of the spinal cord that co-expresses MafB, Oc1, and Oc2, a defining molecular signature of Renshaw interneurons that mediate the recurrent inhibition of motor neurons (Benito-Gonzalez and Alvarez, 2012; Bikoff et al., 2016; Stam et al., 2012). Intriguingly, our experiments suggest that additional Renshaw cell diversity may exist selectively at limb levels, where three candidate V1 cell types express the Renshaw cell markers—MafA, MafB, Oc1 and/or Oc2 —in diverse combinations.

In addition to potential markers of Ia-inhibitory and Renshaw cell V1 subtypes, we identified many other V1 subtypes that differ along the rostro-caudal axis, including numerous limb- and thoracic-specific subsets of V1 interneurons. Given the low number of hypaxial motor pools at thoracic levels (Smith and Hollyday, 1983), such diversity in thoracic V1 interneurons first appears puzzling. One potential function of thoracic V1 subpopulations may be to coordinate fore- and hind-limb motor neuron firing through long-range axonal projections. Supporting this possibility, axonal projections of V1 interneurons at lumbar levels extend at least two millimeters in both the rostral and caudal direction, spanning many spinal segments and extending into the thoracic spinal cord (Britz et al., 2015). A second possibility is that thoracic V1 interneuron diversity reflects the graded need to control the firing of preganglionic motor neurons, organized along the rostro-caudal axis by their peripheral targets (Anderson et al., 1989).

Evolution and the Specification of V1 interneurons

The finding that V1 interneurons acquire unique segmental identities has implications for the emergence of interneuron diversity during evolution. As organisms transitioned from water-to land-based movement, spinal circuits adapted to control an expanded number of muscles with new biomechanical constraints, including the need to regulate flexion/extension at limb levels and breathing, balance and posture at thoracic levels.

In a single organism, *Xenopus laevis*, this evolutionary transition from water to land is recapitulated during metamorphosis. Pre-metamorphosis, the tadpole spinal cord contains few motor neurons, with those present adopting an MMC-like molecular profile and projecting to axial musculature (Roberts et al., 2010). During metamorphosis, as limbs emerge and the number and diversity of motor neurons increases, V1 interneurons appear to exhibit a dramatic expansion in number and diversity (Sweeney et al., unpublished observation). The segmental diversity of V1 interneurons evident in mouse may therefore represent a conserved vertebrate evolutionary strategy to accommodate the appearance of limbs and the transition from water to land.

STAR METHODS

Contact for Reagent and Resource Sharing

Further information and requests for resources and reagents should be directed to and will be fulfilled by the Lead Contact, Thomas Jessell (tmj1@cumc.columbia.edu).

Experimental Model and Subject Details

The following previously published mouse strains were used in this study: *En1::Cre* (Kimmel et al., 2000; Sapir et al., 2004), *Tau.lsl.mGFP.IRES.nLacZ* (Hippenmeyer et al., 2005), *Olig2::Cre* (Dessaud et al 2007) and *Hoxc9*$^{-/-}$ (Jung et al 2014, McIntyre et al 2007). Wildtype and experimental mice were maintained on a C57Bl/6 (*En1::Cre, Tau.lsl.mGFP.IRES.nLacZ, Olig2::Cre)* or mixed (*Hoxc9*$^{-/-}$) genetic background. Male and female mice were both used depending on availability, and were maintained using standard husbandry and housing conditions. All experiments and procedures were performed according to NIH guidelines and approved by the Institutional Animal Care and Use Committee of Columbia University or New York University.

Method Details

Immunohistochemistry—Immunohistochemistry for e18.5-p0 was performed on mice transcardially perfused with 4% paraformaldehyde in 0.1M phosphate buffer, followed by a 2 hour post-fixation. Embryonic spinal cords at e14.5 were fixed in 4% paraformaldehyde in phosphate buffer for 1 hour at 4°C. Fixed tissue was washed, cryoprotected by equilibration in 30% sucrose in 0.1M phosphate buffer, embedded in OCT, frozen on dry ice, and cryostat-sectioned in the transverse plane at 12 μm. Tissue sections from p0 mice were collected at C3-8 (brachial), T4-11 (thoracic), and L2-6 (lumbar), unless otherwise noted. At e14.5, sections from brachial, thoracic and lumbar levels were confirmed with FoxP1/Raldh2 staining of LMC motor neurons.

Immunohistochemistry was performed on tissue through sequential exposure to primary antibodies overnight at 4°C, and fluorophore-conjugated (Alexa Fluor 405, DyLight 488 or Alexa Fluor 488, Alex Fluor 549 or Cy3, and Alexa Fluor 647 or Cy5) secondary antibodies for 30 minutes at room temperature. Sections were mounted using Vectashield or PVA/DABCO and coverslipped for imaging. Confocal images were obtained on a LSM 710 or 780 Confocal microscope (Carl Zeiss) at 512×512 resolution, using a Plan-Apochromat 20×/0.8 M27 objective.

For this study, we generated the following antibody, along with its corresponding antigen and working concentration: chicken anti-β-Galactosidase against lyophilized β-Galactosidase powder (Sigma 48275, 1:16000). Antibodies generously provided as gifts include: rabbit anti-Nr3b2, from Jeremy Nathans (1:2000; Chen and Nathans, 2007); rat (1:10000) anti-Bhlhb5 and rabbit (1:5000)/guinea pig (1:20000) anti-Prdm8, from Sarah Ross (Ross et al., 2010; Ross et al., 2012). Antibodies used as previously described (Bikoff et al., 2016) include: guinea pig anti-FoxP2: DAGSRDGRSSGDTSSEVSTVC (1:20000); rabbit anti-FoxP4: ASSLLPLSQEDLGVPGEP (1:64000); guinea pig anti-Lmo3: EEGLMKEGYAPQVR (1:8000); rat anti-MafA: CGFPREPSPAQAGPGAAKGAPD

(1:4000); guinea pig anti-Nr3b2: amino acids 186-237 from mouse Nr3b2 (1:16000); rat anti-Nr4a2: SGEYSSDFLTPEFVKFSMDC (1:10000); rat (1:4000)/rabbit (1:4000) anti-Nr5a2: GYQPYGHFPSRAIKSEY/LPPTDYDRSPFVTSP; guinea pig (1:32000)/rat (1:4000) anti-Otp: DPGGHPGDLAPNSDPVEGATC; guinea pig anti-Pou6f2: LRGEDKAATSDSELNE (1:4000); guinea pig (1:32000)/rat (1:16000) anti-Pou6f2: mouse protein corresponding to amino acids 35-184 of human Pou6f2; guinea pig (1:16000)/rat (1:16000) anti-Prdm8: amino acids 228-457 from mouse Prdm8; and rat (1:4000) anti-Sp8: CPELLQPPEPGHRNGLE.

Other antibodies used in this study include: goat anti-Bhlhb5 (beta-3) (1:2000, Santa Cruz, clone E-17); chick anti-β-Galactosidase (1:5000, Abcam, ab9361); rabbit (1:2000, Swant, CB38) and mouse (1:500, Swant, 300) anti-Calbindin D28K; rabbit or guinea pig anti-FoxP1 (1:20000, Jessell Lab); goat anti-FoxP2 (1:500, Santa Cruz, clone N-16); guinea pig anti-Hoxc6 (1:16000, Jessell Lab); guinea pig anti-Hoxc9 (1:64000, Jung et al., 2010); rabbit anti-MafA (1:2000, Novus Biologicals, NB400-137); rabbit anti-MafB (1:2000, Sigma, HPA005653); mouse anti-Nr3b3 (Err3) (1:2000, R&D Systems, PP-H6812-00);rabbit anti-Nr4a2 (Nurr1) (1:500, Santa Cruz, clone M-196); goat anti-Nr5a2 (1:100, Santa Cruz, clone C-17); rabbit anti-Onecut1 (HNF-6) (1:2000, Santa Cruz, clone H-100); rabbit anti-Onecut1 (1:200, Sigma, HPA003457); sheep anti-Onecut2 (1:2000, R&D Systems, AF6294); rabbit anti-Otp (1:2000, Abcam, AB-50897); rabbit anti-Pou6f2 (1:2000, Sigma, HPA008699); rabbit anti-Prox1 (1:2000, Millipore, AB5475); rabbit anti-Raldh2 (1:8000, Jessell Lab); goat anti-Sp8 (1:2000, Santa Cruz, clone C-18); rabbit anti-Sp8 (1:20000, Millipore, AB-15260) and rabbit anti-Zfhx4 (1:2000, Sigma, HPA023837, lot G105409).

Analysis of Transcription Factor Co-expression—To estimate the fraction of the parental V1 population labeled by our transcription factors, we simultaneously applied antibodies against the 19 transcription factors (Bhlhb5, FoxP1, FoxP2, FoxP4, Lmo3, MafA, MafB, Nr3b2, Nr3b3, Nr4a2, Nr5a2, Oc1, Oc2, Otp, Pou6f2, Prdm8, Prox1, Sp8 and Zfhx4) to sections from *En1::Cre; Tau.lsl.nLacZ* mice, in which V1 interneurons are marked by expression of nLacZ.

To assess transcription factor co-expression, confocal images were imported into Imaris (Bitplane), and analyzed using the "Spots" and "Colocalization" functions, followed by manual validation. Thresholds were set to exclude nonspecific background immunoreactivity. Variations in levels of expression were not taken into consideration, resulting in a determination of either "co-expressed" or "not co-expressed". For each transcription factor combination, we analyzed two or more lumbar sections from at least two p0 animals (see Table S1).

Analysis of Interneuron Spatial Distributions—For the lumbar, thoracic, and cervical spinal segments of e14.5, e18.5 and p0 mice, the position of V1 interneurons was analyzed as previously described (Bikoff et al., 2016; Gabitto et al., 2016). The nucleus of each interneuron was assigned a spot using the "Spots" function in Imaris (Bitplane) and Cartesian coordinates for each interneuron were determined in the transverse spinal cord plane with respect to the midpoint of the central canal, defined as position (0,0). For the thoracic spinal cord, sections were normalized to a standardized hemi-section that reflected

the narrower shape of the spinal cord, as measured in Imaris. The distance from central canal to lateral boundary was 650 μm for lumbar and 450 μm for thoracic hemi-segments; the distance from central canal to bottom-most boundary was 400 μm for thoracic and lumbar hemi-segments. The brachial spinal cord was morphed to the lumbar spinal cord size and shape.

Bayesian Sparse Regression Model—Samples from the posterior distribution of the Bayesian sparse regression model conditioned on the thoracic dataset were obtained as in Gabitto et al., 2016, using expression and co-expression fractional values and single transcription factors spatial distributions. Clade diagrams were drawn by considering FoxP2, Sp8, MafA and Pou6f2 as the mutually exclusive TFs of the first level of the hierarchy permitting comparison with lumbar results. This set of transcription factors remains mutually exclusive at thoracic levels.

Quantification and Statistical Analysis—All statistical details are described in figure legends, Table S1, or Methods S1. Significance between means was assessed with an unpaired two-tailed Student's T-test for thoracic v. lumbar comparisons, or an ANOVA followed by a Bonferroni's test for multiple comparisons. All data represent mean ± SEM unless noted.

Supplementary Material

Refer to Web version on PubMed Central for supplementary material.

Acknowledgments

References

Agalliu D, Takada S, Agalliu I, McMahon AP, Jessell TM. Motor neurons with axial muscle projections specified by Wnt4/5 signaling. Neuron. 2009; 61:708–720. [PubMed: 19285468]

Alvarez FJ, Jonas PC, Sapir T, Hartley R, Berrocal MC, Geiman EJ, Todd AJ, Goulding M. Postnatal phenotype and localization of spinal cord V1 derived interneurons. J Comp Neurol. 2005; 493:177–192. [PubMed: 16255029]

Anderson CR, McLachlan EM, Srb-Christie O. Distribution of sympathetic preganglionic neurons and monoaminergic nerve terminals in the spinal cord of the rat. J Comp Neurol. 1989; 283:269–284. [PubMed: 2567744]

Baek M, Pivetta C, Liu JP, Arber S, Dasen JS. Columnar-Intrinsic Cues Shape Premotor Input Specificity in Locomotor Circuits. Cell Rep. 2017; 21:867–877. [PubMed: 29069594]

Benito-Gonzalez A, Alvarez FJ. Renshaw cells and Ia inhibitory interneurons are generated at different times from p1 progenitors and differentiate shortly after exiting the cell cycle. J Neurosci. 2012; 32:1156–1170. [PubMed: 22279202]

Bikoff JB, Gabitto MI, Rivard AF, Drobac E, Machado TA, Miri A, Brenner-Morton S, Famojure E, Diaz C, Alvarez FJ, et al. Spinal Inhibitory Interneuron Diversity Delineates Variant Motor Microcircuits. Cell. 2016; 165:207–219. [PubMed: 26949184]

Britz O, Zhang J, Grossmann KS, Dyck J, Kim JC, Dymecki S, Gosgnach S, Goulding M. A genetically defined asymmetry underlies the inhibitory control of flexor-extensor locomotor movements. Elife. 2015; 4:147.

Cadwell CR, Palasantza A, Jiang X, Berens P, Deng Q, Yilmaz M, Reimer J, Shen S, Bethge M, Tolias KF, et al. Electrophysiological, transcriptomic and morphologic profiling of single neurons using Patch-seq. Nat Biotechnol. 2016; 34:199–203. [PubMed: 26689543]

Campbell JN, Macosko EZ, Fenselau H, Pers TH, Lyubetskaya A, Tenen D, Goldman M, Verstegen AMJ, Resch JM, McCarroll SA, et al. A molecular census of arcuate hypothalamus and median eminence cell types. Nat Neurosci. 2017; 20:484–496. [PubMed: 28166221]

Catela C, Shin MM, Dasen JS. Assembly and function of spinal circuits for motor control. Annu Rev Cell Dev Biol. 2015; 31:669–698. [PubMed: 26393773]

Dasen JS, Jessell TM. Hox networks and the origins of motor neuron diversity. Curr Top Dev Biol. 2009; 88:169–200. [PubMed: 19651305]

Dasen JS, De Camilli A, Wang B, Tucker PW, Jessell TM. Hox repertoires for motor neuron diversity and connectivity gated by a single accessory factor, FoxP1. Cell. 2008; 134:304–316. [PubMed: 18662545]

Dasen JS, Liu JP, Jessell TM. Motor neuron columnar fate imposed by sequential phases of Hox-c activity. Nature. 2003; 425:926–933. [PubMed: 14586461]

Dasen JS, Tice BC, Brenner-Morton S, Jessell TM. A Hox regulatory network establishes motor neuron pool identity and target-muscle connectivity. Cell. 2005; 123:477–491. [PubMed: 16269338]

De Marco Garcia NV, Jessell TM. Early motor neuron pool identity and muscle nerve trajectory defined by postmitotic restrictions in Nkx6.1 activity. Neuron. 2008; 57:217–231. [PubMed: 18215620]

Dessaud E, Yang LL, Hill K, Cox B, Ulloa F, Ribeiro A, Mynett A, Novitch BG, Briscoe J. Interpretation of the sonic hedgehog morphogen gradient by a temporal adaptation mechanism. Nature. 2007; 450:717–720. [PubMed: 18046410]

Eccles JC, Fatt P, KOKETSU K. Cholinergic and inhibitory synapses in a pathway from motor-axon collaterals to motoneurones. J Physiol (Lond). 1954; 126:524–562. [PubMed: 13222354]

Eccles RM, Lundberg A. Integrative pattern of Ia synaptic actions on motoneurones of hip and knee muscles. J Physiol (Lond). 1958; 144:271–298. [PubMed: 13611693]

Francius C, Harris A, Rucchin V, Hendricks TJ, Stam FJ, Barber M, Kurek D, Grosveld FG, Pierani A, Goulding M, et al. Identification of multiple subsets of ventral interneurons and differential distribution along the rostrocaudal axis of the developing spinal cord. PLoS ONE. 2013; 8:e70325. [PubMed: 23967072]

Friese A, Kaltschmidt JA, Ladle DR, Sigrist M, Jessell TM, Arber S. Gamma and alpha motor neurons distinguished by expression of transcription factor Err3. Proc Natl Acad Sci USA. 2009; 106:13588–13593. [PubMed: 19651609]

Gabitto MI, Pakman A, Bikoff JB, Abbott LF, Jessell TM, Paninski L. Bayesian Sparse Regression Analysis Documents the Diversity of Spinal Inhibitory Interneurons. Cell. 2016; 165:220–233. [PubMed: 26949187]

Goulding M. Circuits controlling vertebrate locomotion: moving in a new direction. Nat Rev Neurosci. 2009; 10:507–518. [PubMed: 19543221]

Grillner S, Jessell TM. Measured motion: searching for simplicity in spinal locomotor networks. Curr Opin Neurobiol. 2009; 19:572–586. [PubMed: 19896834]

Grossmann KS, Giraudin A, Britz O, Zhang J, Goulding M. Genetic dissection of rhythmic motor networks in mice. Prog Brain Res. 2010; 187:19–37. [PubMed: 21111198]

Hultborn H, Jankowska E, Lindström S. Recurrent inhibition of interneurones monosynaptically activated from group Ia afferents. J Physiol (Lond). 1971; 215:613–636. [PubMed: 4253675]

Jankowska E, Odutola A. Crosses and uncrossed synaptic actions on motoneurones of back muscles in the cat. Brain Res. 1980; 194:65–78. [PubMed: 6445769]

Jung H, Lacombe J, Mazzoni EO, Liem KF, Grinstein J, Mahony S, Mukhopadhyay D, Gifford DK, Young RA, Anderson KV, et al. Global control of motor neuron topography mediated by the repressive actions of a single hox gene. Neuron. 2010; 67:781–796. [PubMed: 20826310]

Jung H, Mazzoni EO, Soshnikova N, Hanley O, Venkatesh B, Duboule D, Dasen JS. Evolving Hox activity profiles govern diversity in locomotor systems. Dev Cell. 2014; 29:171–187. [PubMed: 24746670]

Kirkwood PA, Sears TA, Westgaard RH. Recurrent inhibition of intercostal motoneurones in the cat. J Physiol (Lond). 1981; 319:111–130. [PubMed: 7320908]

Lacombe J, Hanley O, Jung H, Philippidou P, Sürmeli G, Grinstein J, Dasen JS. Genetic and functional modularity of Hox activities in the specification of limb-innervating motor neurons. PLoS Genet. 2013; 9:e1003184. [PubMed: 23359544]

Landmesser L. The distribution of motoneurones supplying chick hind limb muscles. J Physiol (Lond). 1978; 284:371–389. [PubMed: 731549]

Lin JH, Saito T, Anderson DJ, Lance-Jones C, Jessell TM, Arber S. Functionally related motor neuron pool and muscle sensory afferent subtypes defined by coordinate ETS gene expression. Cell. 1998; 95:393–407. [PubMed: 9814709]

Lipski J, Fyffe RE, Jodkowski J. Recurrent inhibition of cat phrenic motoneurons. J Neurosci. 1985; 5:1545–1555. [PubMed: 4009244]

McIntyre DC, Rakshit S, Yallowitz AR, Loken L, Jeannotte L, Capecchi MR, Wellik DM. Hox patterning of the vertebrate rib cage. Development. 2007; 134:2981–2989. [PubMed: 17626057]

Mendelsohn AI, Dasen JS, Jessell TM. Divergent Hox Coding and Evasion of Retinoid Signaling Specifies Motor Neurons Innervating Digit Muscles. Neuron. 2017; 93:792–805.e794. [PubMed: 28190640]

Novitch BG, Chen AI, Jessell TM. Coordinate regulation of motor neuron subtype identity and pan-neuronal properties by the bHLH repressor Olig2. Neuron. 2001; 31:773–789. [PubMed: 11567616]

Philippidou P, Dasen JS. Hox genes: choreographers in neural development, architects of circuit organization. Neuron. 2013; 80:12–34. [PubMed: 24094100]

Renshaw B. Influence of discharge of motoneurons upon excitation of neighboring motoneurons. J Neurophysiol. 1941; 4:167–183.

Roberts A, Li WC, Soffe SR. How neurons generate behavior in a hatchling amphibian tadpole: an outline. Front Behav Neurosci. 2010; 4:16. [PubMed: 20631854]

Romanes GJ. The motor cell columns of the lumbo-sacral spinal cord of the cat. J Comp Neurol. 1951; 94:313–363. [PubMed: 14832391]

Rousso DL, Gaber ZB, Wellik D, Morrisey EE, Novitch BG. Coordinated actions of the forkhead protein Foxp1 and Hox proteins in the columnar organization of spinal motor neurons. Neuron. 2008; 59:226–240. [PubMed: 18667151]

Sears TA. Some Properties and Reflex Connexions of Respiratory Motoneurones of the Cat's Thoracic Spinal Cord. J Physiol (Lond). 1964; 175:386–403. [PubMed: 14241839]

Smith CL, Hollyday M. The development and postnatal organization of motor nuclei in the rat thoracic spinal cord. J Comp Neurol. 1983; 220:16–28. [PubMed: 6315781]

Sockanathan S, Jessell TM. Motor neuron-derived retinoid signaling specifies the subtype identity of spinal motor neurons. Cell. 1998; 94:503–514. [PubMed: 9727493]

Sockanathan S, Perlmann T, Jessell TM. Retinoid receptor signaling in postmitotic motor neurons regulates rostrocaudal positional identity and axonal projection pattern. Neuron. 2003; 40:97–111. [PubMed: 14527436]

Stam FJ, Hendricks TJ, Zhang J, Geiman EJ, Francius C, Labosky PA, Clotman F, Goulding M. Renshaw cell interneuron specialization is controlled by a temporally restricted transcription factor program. Development. 2012; 139:179–190. [PubMed: 22115757]

Tasic B, Menon V, Nguyen TN, Kim TK, Jarsky T, Yao Z, Levi B, Gray LT, Sorensen SA, Dolbeare T, et al. Adult mouse cortical cell taxonomy revealed by single cell transcriptomics. Nat Neurosci. 2016; 19:335–346. [PubMed: 26727548]

Wallace ML, Saunders A, Huang KW, Philson AC, Goldman M, Macosko EZ, McCarroll SA, Sabatini BL. Genetically Distinct Parallel Pathways in the Entopeduncular Nucleus for Limbic and Sensorimotor Output of the Basal Ganglia. Neuron. 2017; 94:138–152.e5. [PubMed: 28384468]

Zagoraiou L, Akay T, Martin JF, Brownstone RM, Jessell TM, Miles GB. A cluster of cholinergic premotor interneurons modulates mouse locomotor activity. Neuron. 2009; 64:645–662. [PubMed: 20005822]

Zeisel A, Muñoz-Manchado AB, Codeluppi S, Lönnerberg P, La Manno G, Juréus A, Marques S, Munguba H, He L, Betsholtz C, et al. Brain structure. Cell types in the mouse cortex and hippocampus revealed by single-cell RNA-seq. Science. 2015; 347:1138–1142. [PubMed: 25700174]

Zhang J, Lanuza GM, Britz O, Wang Z, Siembab VC, Zhang Y, Velasquez T, Alvarez FJ, Frank E, Goulding M. V1 and v2b interneurons secure the alternating flexor-extensor motor activity mice require for limbed locomotion. Neuron. 2014; 82:138–150. [PubMed: 24698273]
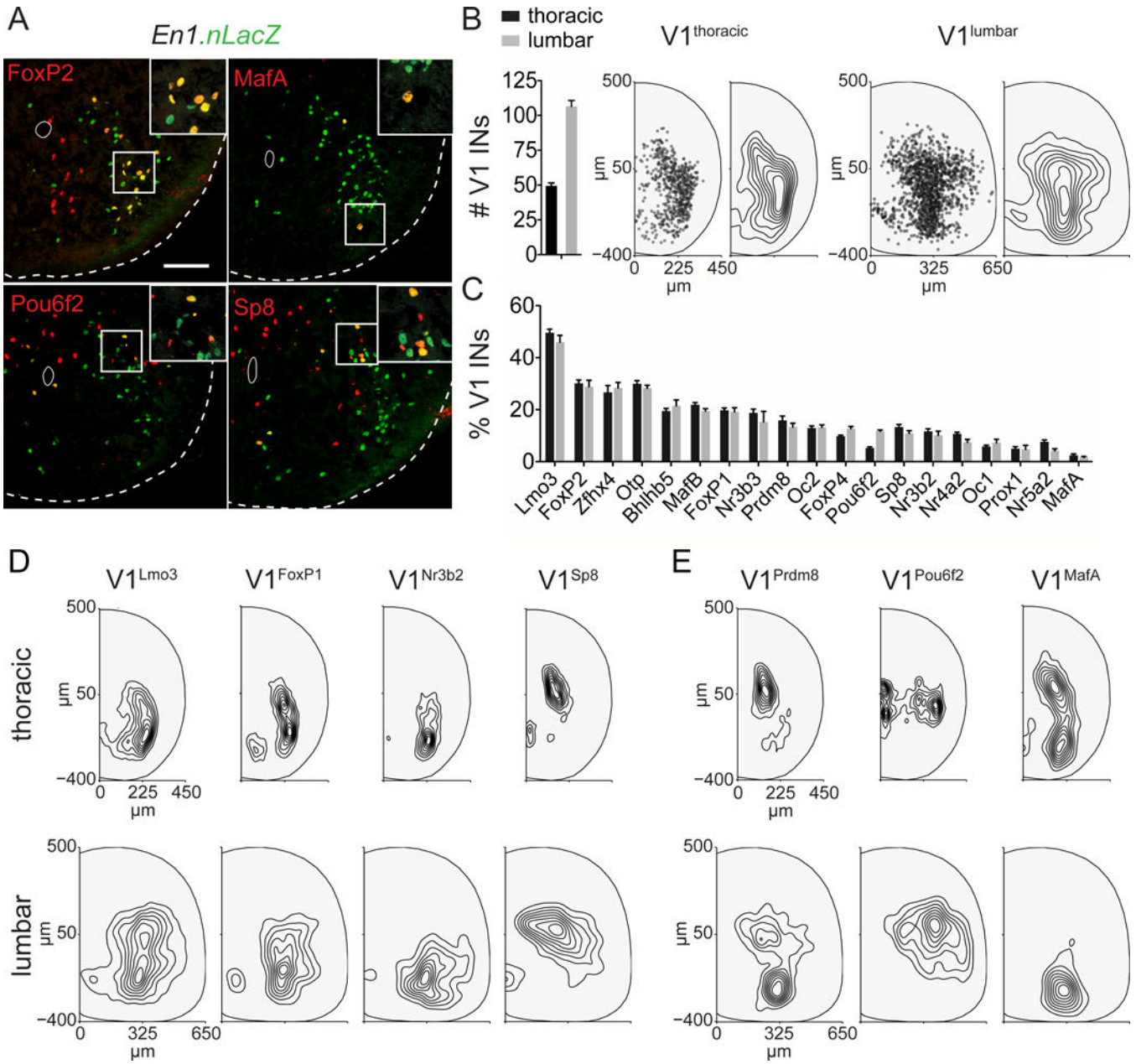
Figure 1. Comparison of Lumbar and Thoracic V1 Interneuron Subpopulations Expressing Single Transcription Factors

(A) Antibodies against FoxP2, MafA, Pou6f2 and Sp8 transcription factors (red) label subsets of V1 interneurons (green) in thoracic spinal segments of p0 *En1.nLacZ* mice. Shown is a ventral hemi-section of spinal cord with the central canal (white circle) and outer edge (dotted line) indicated. Scale bar = 100 μm.

(B) Number and position of V1 interneurons at thoracic (T4-11) or lumbar (L2-6) levels of p0 *En1.nLacZ* mouse spinal cord. Left, number of V1 interneurons per 12 μm hemisection (mean ± SEM for n = 20 animals; p < 0.001 by unpaired t-test). Right, spatial plot of individual cells (left, 50% transparent black to highlight overlap) and 30th-90th percentile density contours (right) from 6 sections/animal for 2 animals.

(C) Percentage of V1 interneurons expressing a given transcription factor at p0 in thoracic (T4-11, black bars) and lumbar (L2-6, gray bars) spinal cord (mean ± SEM for n = 11 animals on average, see Table S1 for detailed n and statistics). $V1^{Pou6f2}$: $p < 0.0001$ for thoracic v. lumbar by unpaired t-test. Only $V1^{Pou6f2}$ exhibits a > 2-fold difference in V1 interneuron number between thoracic and lumbar spinal cord (see also Figure S1A).

(D–E) Comparison of spatial distributions of $V1^{1TF}$ interneurons at thoracic (top, T4-T11) and lumbar (bottom, L2-L6) spinal segments. Shown are examples of representative similar (D) and the most distinct (E) spatial patterns. Contours are ranked from left to right by their level of similarity, defined as the mean cellular displacement required to transform a thoracic spatial distribution into a lumbar distribution (see Figure S1 and Methods S1 for a detailed description of linear transformation and displacement calculations). $\mu(V1^{Lmo3}) = 6.69$ μm; $\mu(V1^{FoxP1}) = 36.04$ μm; $\mu(V1^{Nr3b2}) = 46.57$ μm; $\mu(V1^{Sp8}) = 63.21$ μm; $\mu(V1^{Prdm8}) = 113.54$ μm; $\mu(V1^{Pou6f2}) = 128.92$ μm; $\mu(V1^{MafA}) = 151.20$ μm.
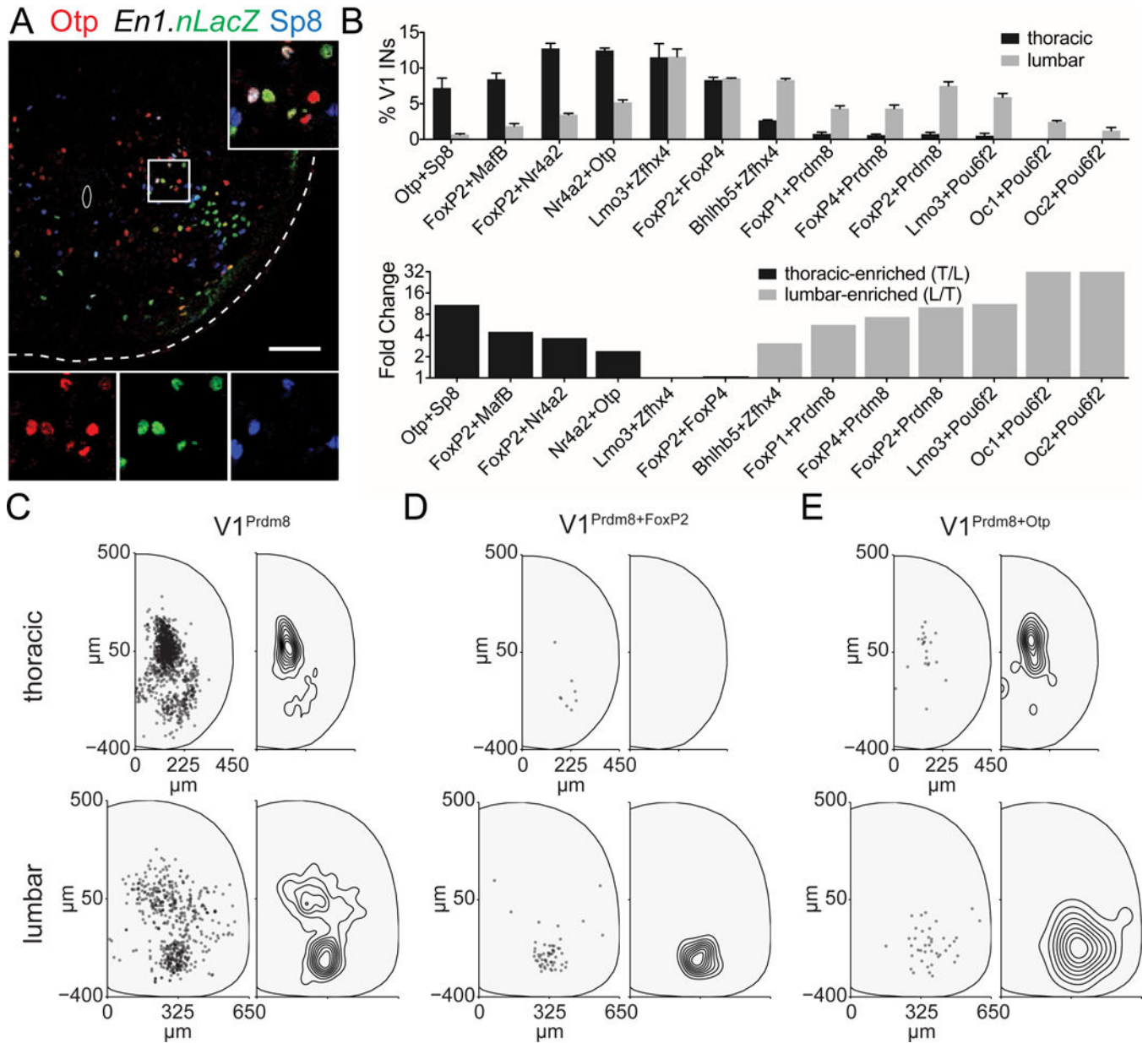
Figure 2. Thoracic- and Limb-Enriched V1 Interneuron Subpopulations Revealed by Coincident Expression of Transcription Factors

(A) Otp (red) and Sp8 (blue) transcription factors mark subsets of V1 interneurons (green) in p0 *En1.nLacZ* thoracic spinal segments. Inset shows V1 interneurons expressing both Otp and Sp8 (white arrows). Scale bar = 100 μm.

(B) Percentage (upper panel) and fold enrichment (lower panel) of V1^{2TF} interneurons with > 2-fold enrichment in thoracic (black) or lumbar (gray) spinal cord (mean ± SEM, n ≥ 2 animals, $p < 0.05$ by unpaired t-test and fold change significance < 0.05—see Table S1 for detailed n and statistics). See also Figure S2 for fold change of other dual- transcription factor combinations with not significant or < 2-fold enrichment.

(C–E) V1 interneurons marked by two transcription factors reveal level-specific spatial domains. Spatial plots of V1^{Prdm8} (C), V1$^{Prdm8 + Foxp2}$ (D) or V1$^{Prdm8 + Otp}$ (E), shown at

thoracic and lumbar levels in the top and bottom panels, respectively. Thoracic level: V1$^{\text{Prdm8+Otp}}$ is more restricted than V1$^{\text{Prdm8}}$ ($\mu = 114$ μm v. $\mu = 224$ μm respectively). Plotted are interneurons in 100 μm of thoracic or lumbar spinal cord from two animals on the left and corresponding contour on the right. Note that no contour is shown in panel D because there are too few cells.
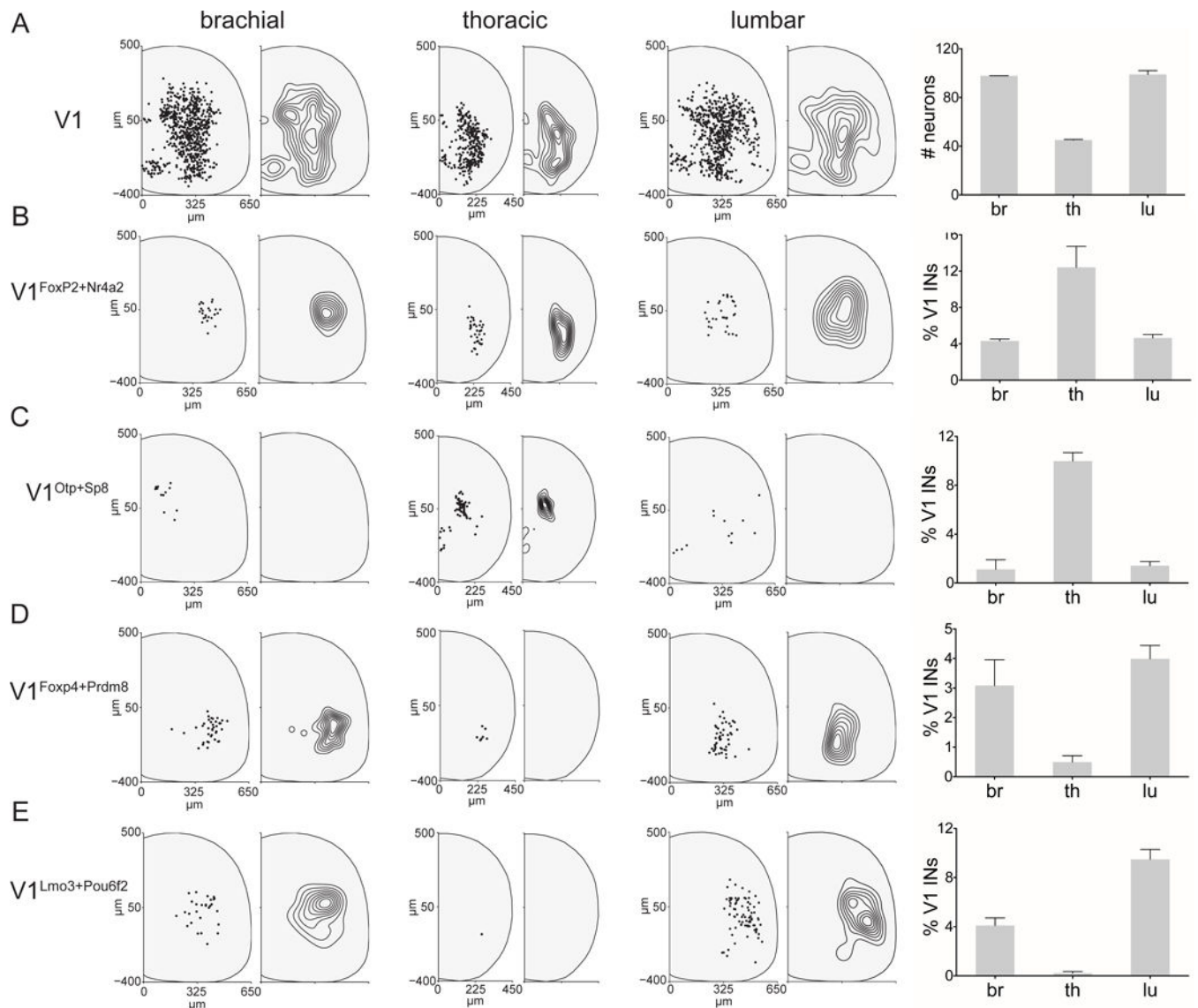
Figure 3. Limb and Thoracic V1 Subpopulations Distinguished By Transcription Factor Expression

(A) Spatial plots, contour profiles, and graph of the number of *En1.nLacZ*[+] V1 interneurons in brachial, thoracic and lumbar p0 spinal cord (mean ± SEM number, $p < 0.0001$ by 1-way ANOVA, brachial or lumbar v. thoracic: $p < 0.05$ by Bonferroni's multiple comparison test).

(B–E) Spatial plots, contour profiles, and graph of ~100 V1 interneurons that also express FoxP2 and Nr4a2 (B), Otp and Sp8 (C), FoxP4 and Prdm8 (D) and Lmo3 and Pou6f2 (E). B: 108 neurons in a 96 μm hemi-segment of C3-5, T4-6, and L3-5 spinal cord containing 30, 43, and 35 neurons respectively. C: 90 neurons in a 156 μm hemi-segment of C6-8, T7-9, and L3-5 spinal cord containing 13, 63, and 14 neurons respectively. D: 97 neurons in a 192 μm hemi-segment of C3-8, T4-9, and L3-5 spinal cord containing 38, 8, and 51 neurons respectively. E: 111 neurons in a 120 μm hemi-segment of C3-5, T4-6, and L3-5 spinal cord containing 29, 1 and 81 neurons respectively. Contours of less than 19 cells cannot be drawn. The right bar graph shows the mean ± SEM percentage (B-E) of V1 interneurons

expressing each marker combination in a 12 μm section. Brachial, lumbar, and thoracic V1 interneuron percentages differ for each combination: $p < 0.0001$ for V1$^{Otp+Sp8}$ and V1$^{Lmo3+Pou6f2}$; $p = 0.0005$ for V1$^{FoxP4+Prdm8}$; $p = 0.0395$ for V1$^{FoxP2+Nr4a2}$ (1-way ANOVA). The percentage of V1 interneurons differs at brachial or lumbar v. thoracic: $p < 0.05$ for V1, V1$^{Otp+Sp8}$, V1$^{FoxP4+Prdm8}$, and V1$^{Lmo3+Pou6f2}$ and $p < 0.10$ for V1$^{FoxP2+Nr4a2}$ (Bonferroni's multiple comparison test). All experiments represent n = 2 to 4 animals (see Table S1 for additional detail).
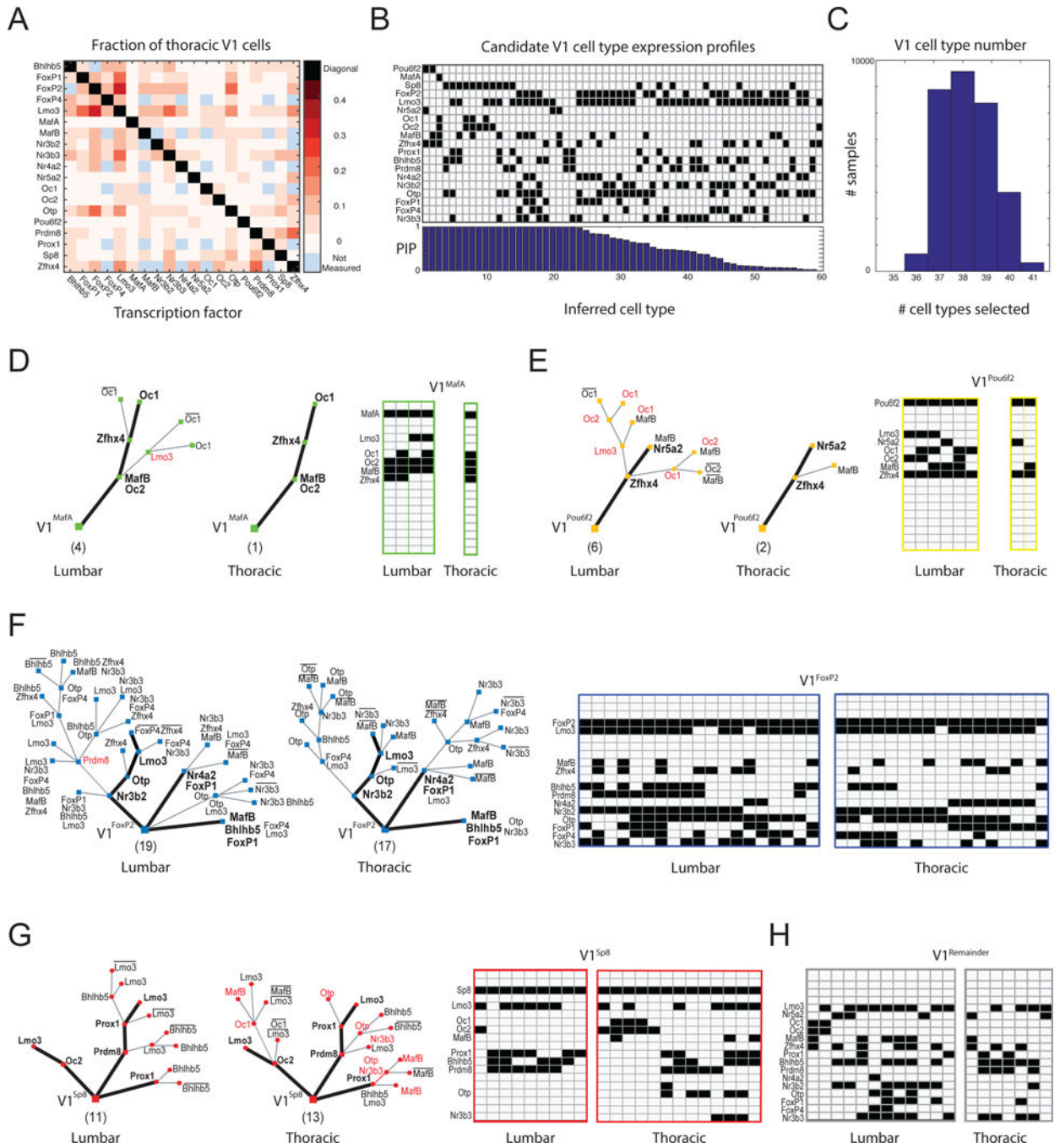
Figure 4. Neuronal Diversity in Lumbar and Thoracic V1 Interneurons Revealed by Bayesian Modeling

(**A**) Fraction of thoracic V1 interneurons labeled by pairs of transcription factors (N.M., Not Measured). Diagonal values represent identity. See Table S1 for additional detail.

(**B**) Expression profiles of top 60 candidate thoracic V1 cell types from all samples with a posterior inclusion probability (PIP) greater than 5%, or 95% confidence. Cell types (top) are arranged by descending posterior inclusion probability (bottom). Black indicates transcription factor expression; white indicates absence of expression.

(C) Number of candidate V1 cell types selected (x-axis) per iteration (sample) of our inference algorithm (y-axis). Cell type expression profile (see Figure 4B) versus cell type number (Figure 4C) are further described in Gabitto et al., 2016.

(D–G) Clade diagram for V1^{MafA} (D), V1^{Pou6f2} (E), V1^{FoxP2} (F) and V1^{Sp8} (G) interneurons, constructed from the mode of the posterior at lumbar and thoracic levels. Note select clade-associated transcription factors are common to both levels (MafA clade: Oc1, Oc2, MafB, and Zfhx4; Pou6f2 clade: Nr5a2, MafB, and Zfhx4; FoxP2 clade: Lmo3, MafB, Zfhx4, Bhlhb5, Nr4a2, Nr3b2, Otp, FoxP1, FoxP4, and Nr3b3; Sp8 clade: Lmo3, Oc2, Prox1, Bhlhb5, and Prdm8), while others are lumbar-specific (MafA clade: Lmo3; Pou6f2: Lmo3, Oc1, Oc2; FoxP2 clade: Prdm8) or thoracic-specific (Sp8 clade: Oc1, MafB, Otp and Nr3b3). Bar above a transcription factor name denotes lack of expression. Bolded lines denote conserved transcription factor combinations present at thoracic and lumbar clades. Red indicates a level-specific transcription factor within a clade. Alongside each clade, expression profiles of candidate cell types from which diagrams are drawn.

(H) Expression profiles of candidate cell types not contained within one of the four clades, V1^{Remainder}, at lumbar and thoracic levels.
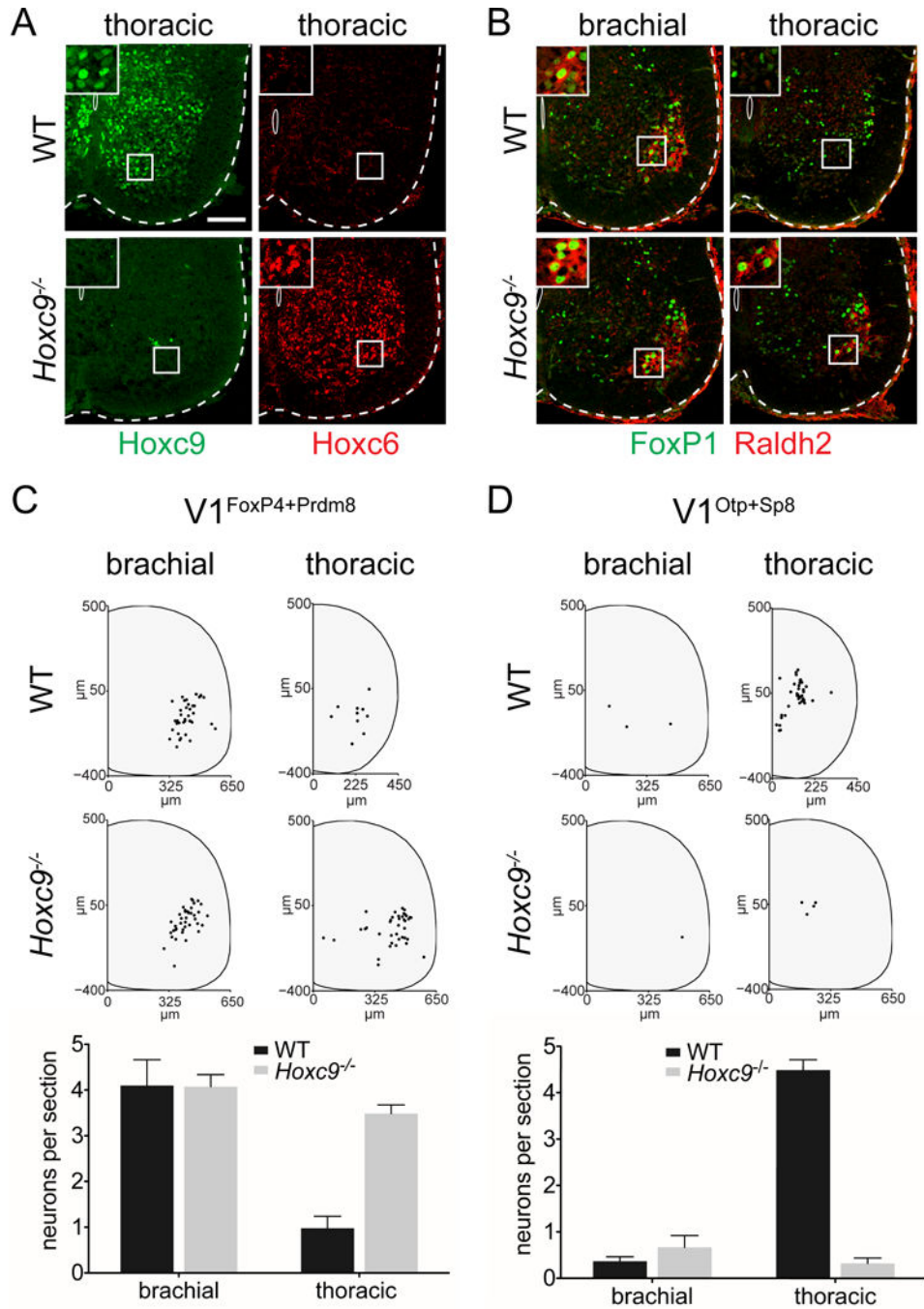
Figure 5. Thoracic to Limb Transformation of V1 Interneurons in *Hoxc9*$^{-/-}$ Mutants

(A) Ventral hemi-section of e14.5 thoracic spinal cord stained for Hoxc9 (green) and Hoxc6 (red) from wildtype (WT; top row) and *Hoxc9*$^{-/-}$ mutant mice (bottom row). Inset shows higher magnification of ventral neurons. Scale bar = 100 μm.

(B) Brachial (left) or thoracic (right) ventral hemi-section of e14.5 spinal cord stained with Foxp1 (green) and the lateral motor column (LMC) marker, Raldh2 (red), in wild type (upper) or *Hoxc9*$^{-/-}$ mutant (bottom) mice. Inset shows higher magnification of ventral neurons. At thoracic levels, FoxP1 expression is still observed in interneurons.

(C–D) Distribution (spatial plots) and number (bar graphs) of neurons that co-express Prdm8 and Foxp4 (C) or Otp and Sp8 (D) within the brachial and thoracic spinal cord in wild type or *Hoxc9*$^{-/-}$ mutant mice at e18.5. *Hoxc9*$^{-/-}$ mutant mice show ectopic expression of limb-enriched markers in thoracic spinal cord (C), while thoracic-enriched subsets are lost (D). Neuron number at brachial levels is unaffected (C-D). Each spinal cord scatterplot displays total cell number per 120 μm of hemi-sections from two animals. Graphs represent mean ± SEM per 12 μm spinal cord hemi-section from 4 to 5 animals (see Table S1 for additional detail). By 2-way ANOVA, $p < 0.01$ comparing either brachial v. thoracic or wildtype v. *Hoxc9*$^{-/-}$ mutant. By Bonferroni's multiple comparison test of brachial v. thoracic, wildtype is significant ($p < 0.001$), but *Hoxc9*$^{-/-}$ mutant is not ($p > 0.05$).
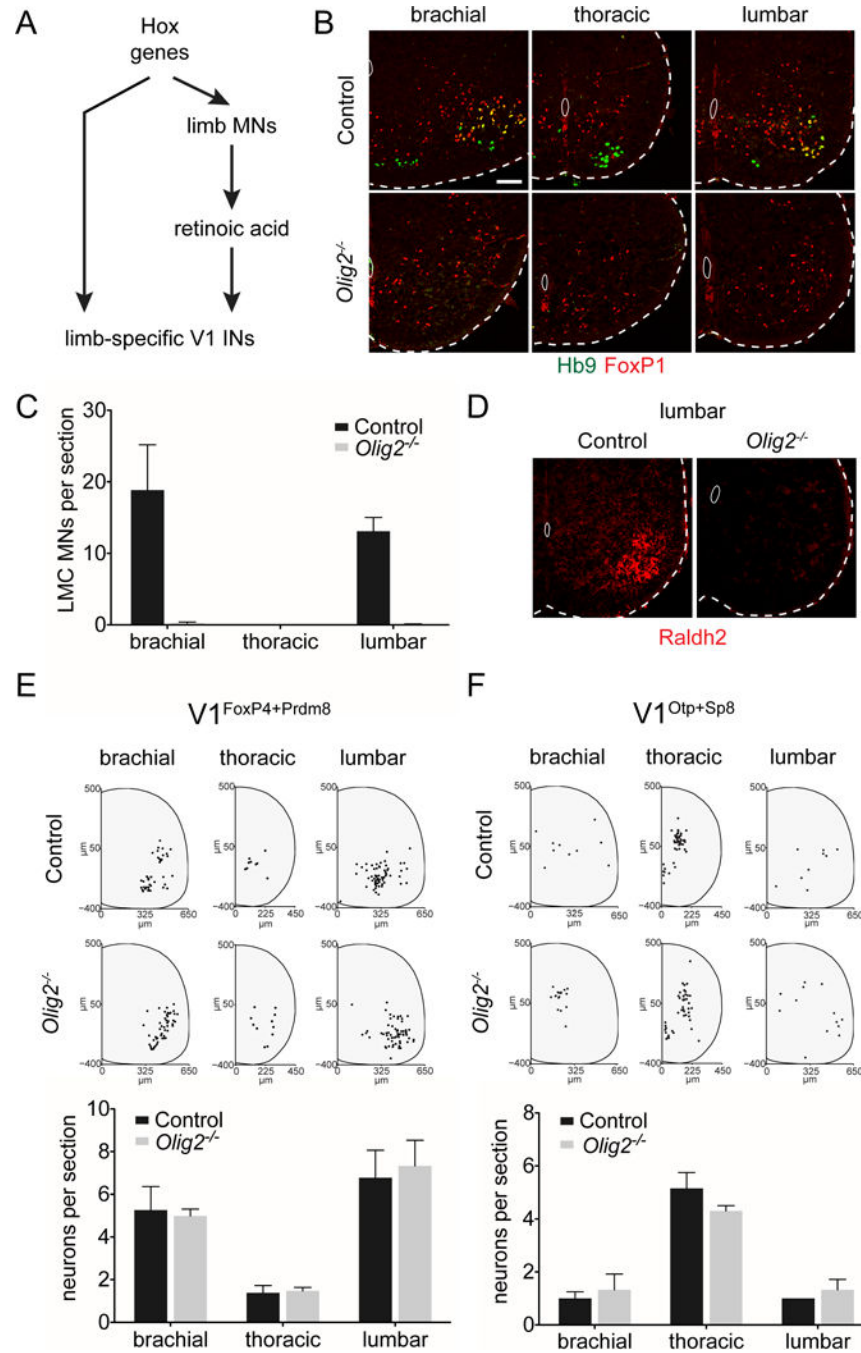
Figure 6. Motor Neuron Elimination Does Not Erode Limb or Thoracic V1 Interneuron Identity
(**A**) Model of *Hox* gene function in V1 interneurons. Left, cell-autonomous *Hox* gene specification of rostro-caudal V1 interneuron identity. Right, non-cell autonomous role for *Hox* genes, acting in LMC motor neurons to initiate production of retinoic acid and subsequent specification of limb-specific V1 interneuron differentiation.
(**B**) Brachial, thoracic and lumbar hemi-sections of the ventral spinal cord stained for Foxp1 (red) and the pan-motor neuron marker, Hb9 (green), in e14.5 control (WT or *Olig2*$^{+/-}$) and *Olig2*$^{-/-}$ mutant mice. Scale bar = 100 μm.

(C) Number of Hb9$^+$ FoxP1$^+$ LMC motor neurons in control (black) or *Olig2*$^{-/-}$ mutant (grey) mice at different segmental levels. Mean ± SEM shown for n = 2 to 4 animals. Motor neuron number differs significantly between control v. *Olig2*$^{-/-}$ mutant based on a 2-way ANOVA (p < 0.0001) or a Bonferroni's multiple comparison test at brachial and lumbar levels (p < 0.01).

(D) Ventral hemi-sections of e18.5 lumbar spinal cord from control (upper panel) and *Olig2*$^{-/-}$ mice (lower panel) stained with the LMC motor neuron marker Raldh2 (red).

(E–F) Spatial distributions (upper panels) and numbers (bar graphs) of V1$^{Prdm8+FoxP4}$ (E) and V1$^{Otp+Sp8}$ (F) interneurons in e18.5 control and *Olig2*$^{-/-}$ mutant mice. Each spinal cord scatterplot displays total cell number per 120 μm hemisection. All data are mean ± SEM for 2 to 7 animals. Level-specific V1 interneurons are not statistically different between control and *Olig2*$^{-/-}$ mutants based on a 2-way ANOVA (p = 0.86).
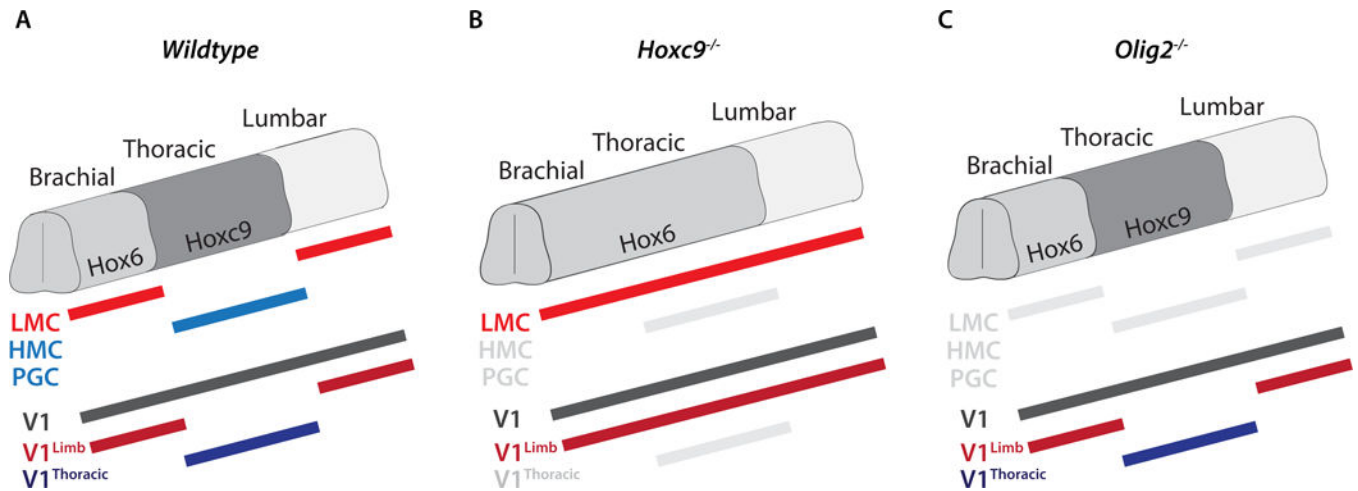
Figure 7. Developmental Origin of V1 Interneuron Diversity

(A) Molecularly distinct subpopulations of V1 interneurons are present at limb (V1Limb) and thoracic (V1Thoracic) levels. This parallels the level-specific identity of motor neurons specified by distinct Hox transcription factor profiles. Limb-innervating motor neurons, expressing Hox6 at brachial levels, form a lateral motor column in the brachial and lumbar spinal cord (LMC, red), and motor neurons innervating the torso and autonomic ganglia in the thoracic spinal cord express Hoxc9 and form a hypaxial and preganglionic column respectively (HMC and PGC, blue).

(B) In the absence of Hoxc9, brachial Hoxc6 extends caudally into the thoracic spinal cord, resulting in the appearance of LMC motor neurons and limb-specific V1 interneurons, and corresponding loss of HMC and PGC motor neurons and thoracic-specific V1 interneurons. Gray color indicates loss of thoracic subtypes.

(C) Loss of Olig2 expression results in the near complete absence of all motor neurons in the developing spinal cord. Motor neuron loss (gray) does not affect the number or distribution of V1Limb and V1Thoracic interneurons.